JOURNAL OF MATERIALS SCIENCE 31 (1996) 6361–6368

Preparation and characterization of PLZT thin films by sol–gel processing

YU-FU KUO, TSEUNG-YUEN TSENG*
Department of Electronics Engineering and Institute of Electronics, National Chiao-Tung University, Hsinchu, Taiwan 30042, Republic of China

The effect of acid catalysts on the sol–gel preparation of ferroelectric lead lanthanum zirconium titanate (PLZT) thin films was studied. High quality thin films were successfully produced by using suitable amounts of the drying control chemical additive formamide and also catalyst acids during the sol–gel processing followed by various annealing conditions. The dielectric constants of the PLZT (8/65/35) thin films produced in this study varied between 540 (100 kHz) for a film annealed at 600 °C for 30 mins to a maximum 870 °C (1 kHz), 700 (100 kHz) for a film annealed at 650 °C for 20 mins.

1. Introduction

In recent years, various physical and chemical methods have been employed to fabricate ferroelectric thin films. These include metal–organic deposition (MOD), chemical vapour deposition (CVD), physical vapour deposition (PVD), liquid phase epitaxy (LPE), and sol–gel processing. Sol–gel processing, which is one of the chemical methods, is a very attractive method. It has many advantages including (1) purity, (2) homogeneity, (3) easier fabrication of a large area thin film at low cost, (4) low temperature processing, (5) ease of forming a variety of structures and (6) ease of controlling stoichiometry, microstructures and film composition. It has been used to prepare ferroelectric thin films for 16 years. It was first used to prepare PLZT thin films by Budd *et al.* in 1985 [1]. Although it has many advantages there are, of course, some disadvantages to this method. The major problems are cracking and porosity created during the drying from the gel to the film and the removal of pore liquids. The cracking problem has been solved by adding drying control chemical additives [2–5]. Only a few attempts at producing pore-free ferroelectric thin films by the sol–gel method have been reported in the literature to date.

The porosity can affect the electrical, piezoelectric, optical and polarization properties of the films [6]. The electrical properties that it may affect include the dielectric constant, the permittivity, the space-charge field and the P–E curve. The space-charge field increases with increasing porosity and the polarization-reversal properties are affected by the space-charge field. As for the piezoelectric properties, it affects the resonant and piezoelectric constants. In the case of the optical properties, when pores exist they may cause light to scatter and thus affect the optical transmittance and refractive index. When pores exist on the surface they may adsorb moisture and impurities that may affect the optical and electrical properties. Thus, it is necessary to eliminate pores in order to obtain the optimal electrical and optical properties for the PLZT thin films. In the present study, we add formamide which acts as a drying control chemical additive (DCCA) in order to prepare crack free ferroelectric thin films and add acid catalysts to prepare pore-free PLZT ferroelectric thin films.

The control of the transformation from the organic precursor solution to an inorganic ceramic film by the pyrolysis process is the key step for avoiding cracking and pores in the film. In order to understand the structural changes occurring during the precursor → sol → gel → crystal transformations, FT–IR spectroscopy and thermogravimetric analysis were used to monitor these transformations. The effect of the formamide and the acid catalyst on the phase transformation will also be discussed.

2. Experimental procedure

Fig. 1 illustrates the flow diagram for the preparation of the stock solutions and the ferroelectric films in a composition range of $Pb_{1-x}La_x(Zr_{1-y}Ti_y)_{1-x/4}O_3$ or PLZT (8/65/35) with an excess of 10 mol % of lead to compensate for the loss of PbO at high temperatures. Lead acetate hydrate, $Pb(CH_3COO)_2 \cdot 3H_2O$, and lanthanum nitrate hydrate, $La(NO_3)_3 \cdot 6H_2O$, were dissolved at 70 °C in 2-methoxyethanol ($CH_3OCH_2CH_2OH$, b.p.: 124.4 °C) and continuously heated at 110 °C for 20 min in order to remove the water. The dehydrated solution was cooled to 90 °C before zirconium *n*-propoxide, $Zr(OC_3H_7)_4$, and titanium *n*-butoxide, $Ti(OC_4H_9)_4$, were added. The solution was raised to its boiling point in order to promote complexation and to remove alkylacetates, which are the

* Author to whom correspondence should be addressed.

0022–2461

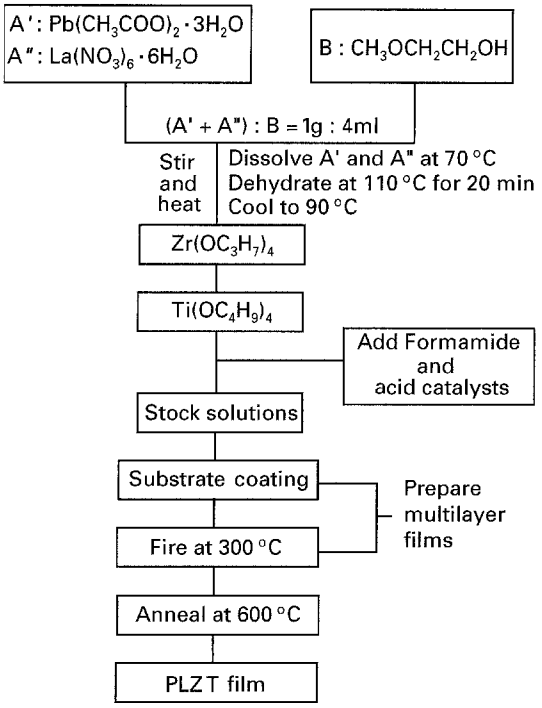

Figure 1 Flow chart of the preparation of thin films by sol–gel processing.

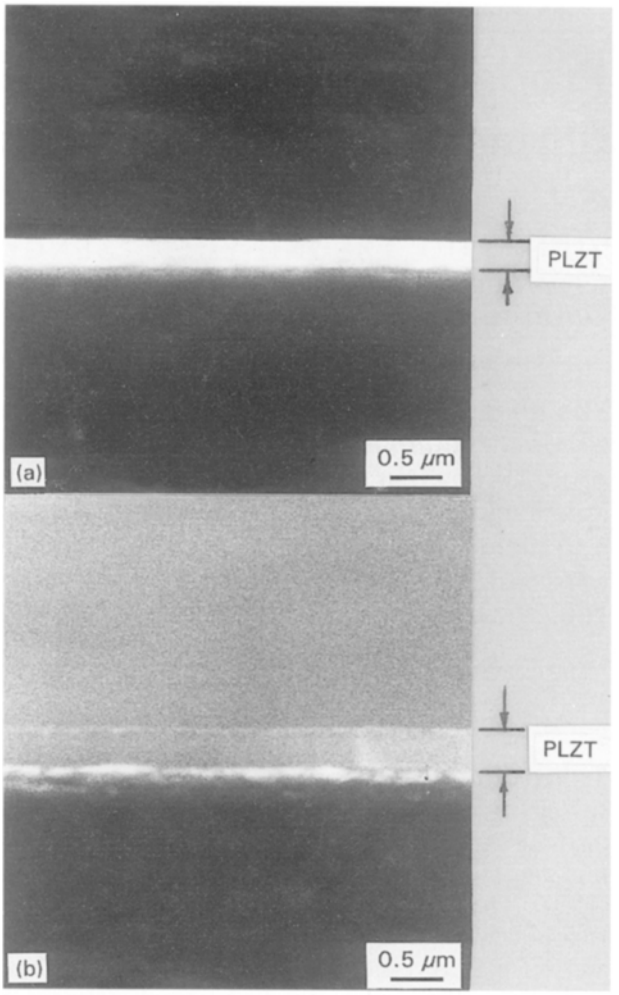

Figure 2 SEM micrographs of the crosssection of PLZT thin films.

by-products of the reaction. Finally, we added formamide (10 vol %), and catalysts (e.g. 0.05 moles of CH_3COOH) to form the stock solution. The concentration of the final solution was 0.714 M. The PLZT (8/65/35) sol–gels were spin coated on to either a cleaned Ti/Si substrate which was prepared by sputtering a 100 nm thickness of titanium on to a silicon wafer or a Pt/Ti/Si substrate which was prepared by first sputtering a 100 nm thickness of titanium and then a 100 nm thickness of platinum onto a silicon wafer. After the spin-coating deposition, the gel films were heat treated at various temperatures and time schedules in an infrared image furnace. The samples were fired at temperatures between 600–650 °C with a heating rate of 5 °C min^{-1}. Thick films were produced by a multiple coating technique. The thickness of the fired sample is about 0.225 μm for one coating and 0.35 μm for two coatings (see Fig. 2).

Thermogravimetric analysis of the gel films were performed using a thermal analyser (SEIKO TG/TGA 200). The heating rate is 10 °C min^{-1} from the firing temperature. The IR spectra were performed using a Nicokt 520 FT–IR spectrometer. The crystalline phase and microstructure of the thin films were characterized by X-ray diffraction (SIEMENS, Diffraktometer D5000) and scanning electron microscopy (SEM, Hitachi model S-2500), respectively. The thickness of the films was observed by using SEM. The dielectric constant was measured by using a HP 4274 LCR meter.

3. Results and discussion

The fabrication process from the precursors to the polycrystalline PLZT ferroelectric thin film can be divided into three transformations: precursor → sol → gel → crystals. The structural changes occuring during these transformations can be monitored by using FTIR spectroscopy. The IR-spectra during the formation of the alkoxide complex are indicated in Fig. 3. The co-solvent, 2-methoxyethanol, has characteristic bands around 1100 cm^{-1} (C–O–C asymmetric absorption), 1420–1330 cm^{-1} (–O–H bending vibration), 2800 cm^{-1} (C–H stretch), 3400 cm^{-1} (O–H stretch) (Fig. 3(a)). After the addition of the lead acetate hydrate, the spectra show two major characteristic bands of the lead acetate hydrate around 1420 cm^{-1} and 1550 cm^{-1} and the characteristic band for Pb–O vibration at around 680 cm^{-1} (Fig. 3(b)). We did not observe any new bands in the acetate region after adding lanthanum nitrates (Fig. 3(c)) and lead acetate hydrate. The sample after the addition of the zirconium *n*-propoxide and the titanium *n*-butoxide shows a new band at around 1740 cm^{-1} (Fig. 3(d) (e)). This proves that there is acetate ester formation.

There are four different types of bonding which exist in this system, they are (1) monodentate, (2) chelation, (3) bridging, and (4) ionic bonding. The symmetric (V_s) and asymmetric stretching vibrations (V_{as}) show characteristic double absorption in the range of 1300–1700 cm^{-1}. Hence FTIR spectroscopy can be utilized for monitoring bonding of the type RCO_2 and metal ions. The difference between the

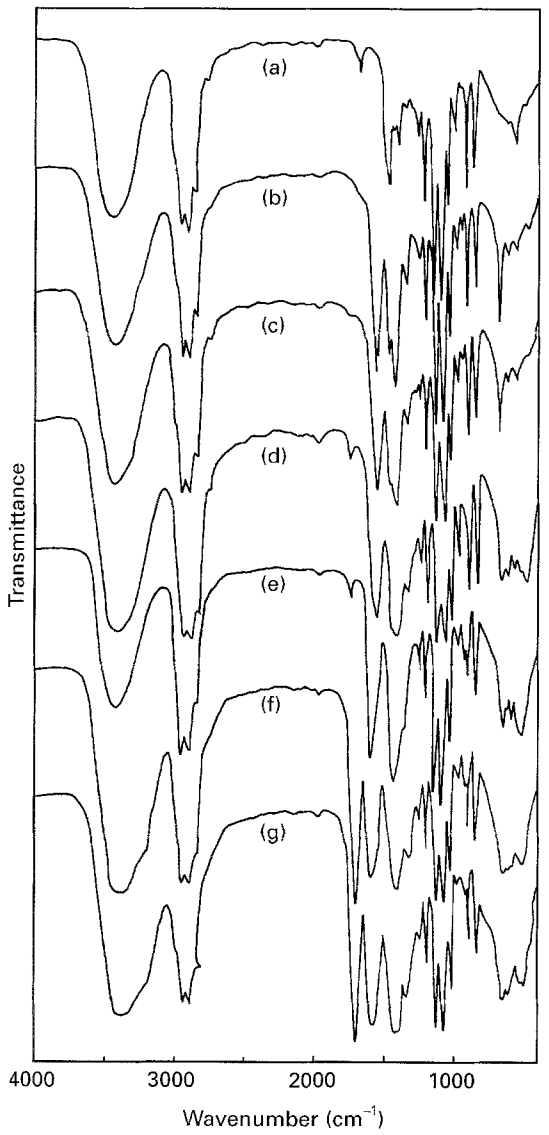

Figure 3 IR-spectra of the formation of the alkoxide complex. (a) M, (b) M + P, (c) M + P + L, (d) M + P + L + Z, (e) M + P + L + Z + T, (f) M + P + L + Z + T + F, (g) M + P + L + Z + T + F + A. Where M = $CH_3OCH_2CH_2OH$, P = $Pb(CH_3COO)_2 \cdot 3H_2O$, L = $La(NO_3)_3 \cdot 6H_2O$, Z = $Zr(OC_3H_7)_4$, T = $Ti(OC_4H_9)_4$, F = formamide, A = CH_3COOH.

characteristic double absorption, ΔV, can be expressed as:

$$\Delta V = V_{as} - V_s$$

The value of ΔV is 425 cm^{-1} for monodentate, 130 cm^{-1} for chelation, 160 cm^{-1} for bridging and 164 cm^{-1} for ionic bonding [7]. The characteristic double absorptions of the acetate are 1420 cm^{-1} (V_s) and 1550 cm^{-1} (V_{as}) with thus a ΔV value of 130 cm^{-1}. Hence the bonding type of the acetate is chelation. Unfortunately Pb, Zr and Ti are heavy atoms so the absorption range is in the far-infrared region. The intensities of the Pb–O, Zr–O, and Ti–O stretching modes, are in the 460–700 cm^{-1} range. The intensities of the characteristic bands from 3100–3600 cm^{-1} showed a marked increase after the addition of the formamide into the solution (Fig. 3(f)). This increase was due to the symmetric stretch absorption of N–H (from 3300–3400 cm^{-1}). The bonding behaviour in formamide is of the resonance type: N–C=O ↔ $^+$N=C–O$^-$, the electron density between the carbon and oxygen would be reduced due to the effect of the partial double-bond behaviour and thus the vibration energy of the C–O bonding will be decreased. The absorption position (1685 cm^{-1}) of the –C=O in formamide would thus shift to lower wavenumbers as compared to the absorption position of –C=O (1710 cm^{-1}) in a system without resonance behaviour. It is found that the absorption position of formamide in the precursor solutions is higher (about 10 cm^{-1}) than in pure formamide. This can be explained by the reduced resonance mode of formamide causing both the number of the C–O bonding and the vibration energy of C–O bonding to increase. The bonding of the unpaired electron on the O or N atoms depends on the kind of bonding modes available when the formamide reacted with other compounds. The formamide chelates with organic-metal molecules and then reacts with H thereby controlling the hydration rate and condensation reaction [8]; therefore, formamide is able to be used as drying control chemical agents. There are no new characteristic bands evident when the acid catalyst (CH_3COOH) was added to the solution (Fig. 3(g)).

Fig. 4 shows the IR spectra of the gel films coated on to the silicon wafer and heat treated at various temperatures for 30 min. Many residual organic compounds exist in the 200 °C heat treated film (Fig. 4(a)). When the annealing temperature was raised to 300 °C,

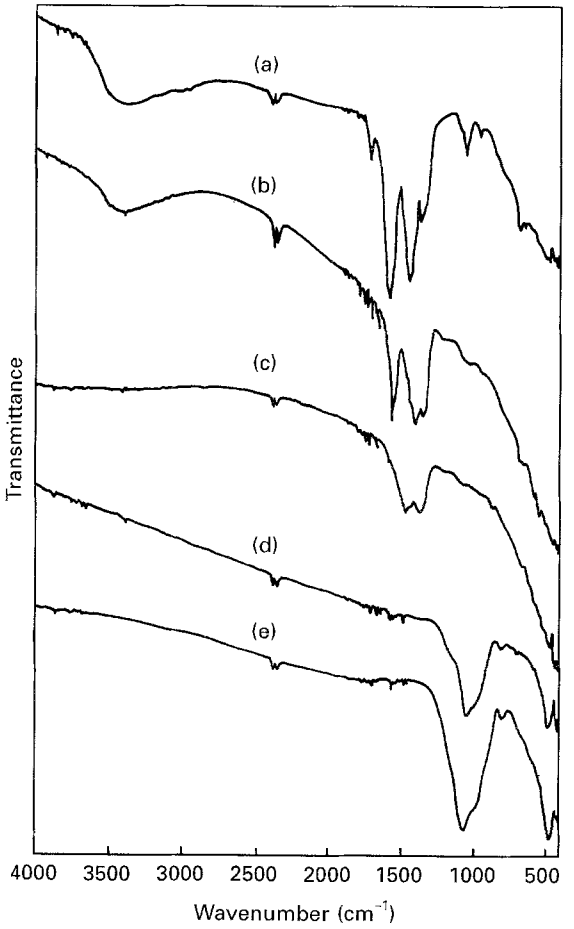

Figure 4 IR-spectra of the gel films coated on the silicon wafer and heat treated at various temperatures for 30 min. with heating rate 10 °C min^{-1}. (a) 200 °C (b) 300 °C (c) 400 °C (d) 500 °C (e) 600 °C.

the characteristic bands around 3200–3600 cm^{-1} become narrower and the absorption peak at 1695 cm^{-1} is eliminated due to the removal of formamide, the residual organic compounds are carboxylate compounds (Fig. 4(b)). For the sample heat treated at 400 °C, the residual carboxylate compounds still remain (Fig. 4(c)). All organic compounds were eliminated at 500 °C and new peaks have appeared at about 1080 cm^{-1} and 800 cm^{-1} which are the characteristic bands of Si–O–Si and O–Si–O, respectively (Fig. 4(d)). The IR spectra indicate that a reaction has occurred between the Si wafer and the PLZT film, and that the PLZT thin film could be a perfect inorganic network structure. The characteristic bands below 500 cm^{-1} are the stretching modes of Pb–O, Ti–O or Zr–O. These characteristic absorption peaks increase with further heat treatment up to 600 °C as is shown in Fig. 4(e).

The transformation of the organic/metal gel film to an inorganic film by pyrolysis involves a large amount of weight loss and volume change during the transformation that is caused by the evaporation of pore liquids. Hence, it is required to carefully control the processing conditions of the pyrolysis if cracks and pores are to be avoided. Thermogravimetric analysis of the gel films is shown in Fig. 5. All the organic is burnt out below 500 °C and there was no further loss in weight beyond this temperature. This result is in good agreement with IR spectra analysis (Fig. 4). On the basis of the analysis of FTIR spectra, most organic materials were eliminated below 200 °C. A small amount of weight loss occurred from 200 °C to 300 °C caused by the removal of formamide and by the decomposition of the carboxylate compound. The weight reduction is rather small from 400 °C to 500 °C. No weight loss occurred for the sample heated above 500 °C.

Fig. 6 shows the SEM micrographs of the PLZT thin films prepared by various forming conditions. The thin film deposited from the sol–gel without the DCCA and the acid catalyst exhibit cracks that occurred during annealing. The non-homogenous pore sizes in the gel film can produce differential evaporation, drying stress and nonuniform surface tension distribution during the removal of pore liquids thus causing the cracking. The DCCA formamide is thus added to the process in an attempt to prepare crack free PLZT films (Fig. 6(b)). The success of the addition of the formamide may be due to a narrowing in the distribution of the pore size, thus minimizing the differential drying stress. This in turn reduces the diffusion length of the metal atoms, leading to the formation of more closed network structures and hence crack-free films at a lower annealing temperature [2, 4]. Some pores however still exist in the films and they will affect the physical properties of the film. Hence, it is necessary to totally eliminate pores in order to obtain high quality thin films.

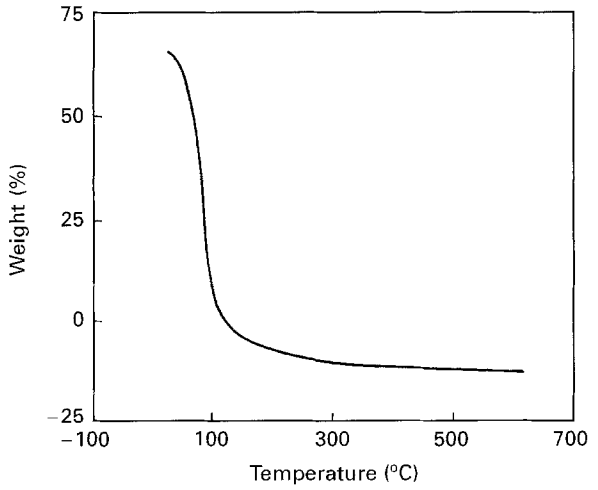

Figure 5 Thermogravimetric analysis of the gel films.

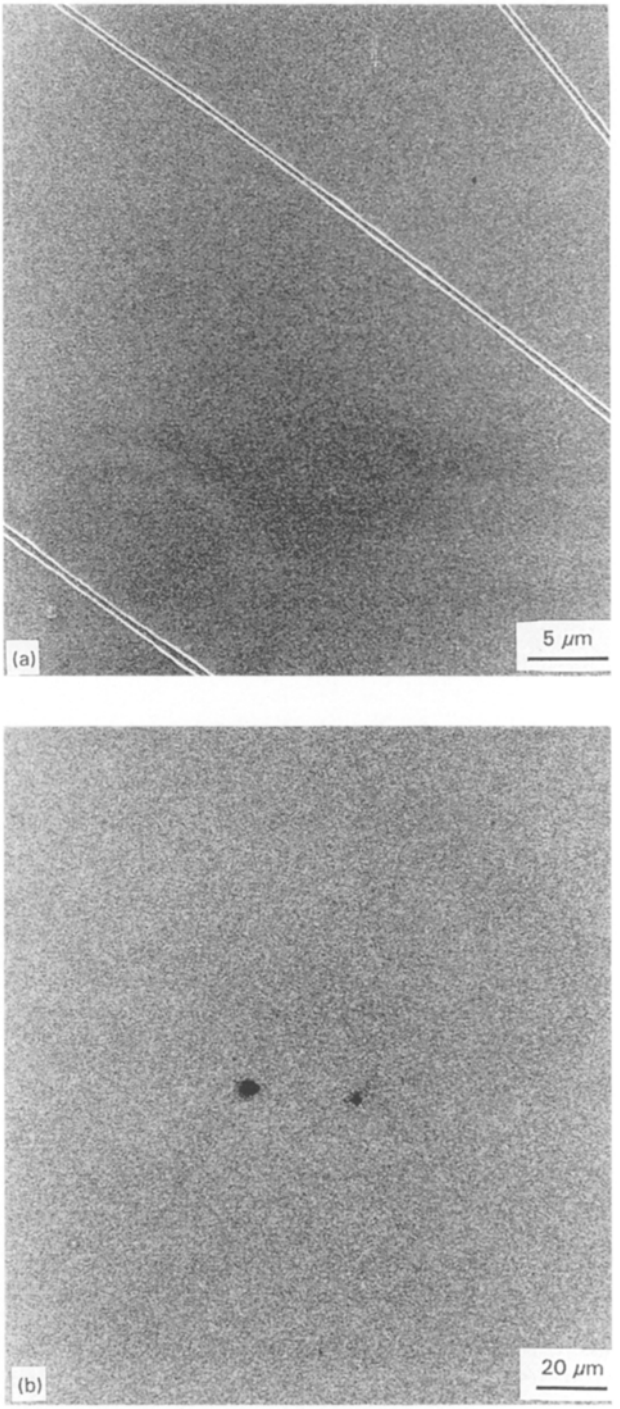

Figure 6 SEM micrographs of the PLZT thin films prepared by various forming conditions: (a) without DCCA and acid catalyst, (b) adding DCCA, (c) adding DCCA and acid catalyst.

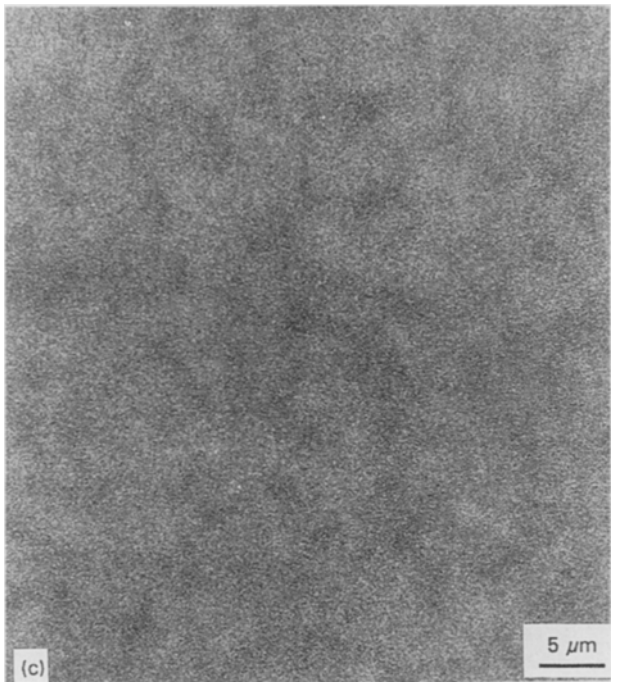

Figure 6 Continued.

The addition of an acid catalyst together with the formamide is thought to have many useful effects including (1) promotion of the hydrolysis through electrophilic reaction and (2) uniform shrinkage during drying [9–10]. The functions of the acid addition are to speed up the hydrolysis reaction rate; and to reduce unreacted M–OR radicals thus subsequently creating more M–OH bonds that leads to a strong gel. In addition it also allows fully hydrolysed monomers to condense thereby maximizing the number of M–O–M bridging bonds and thus creating a high connectivity polymeric structure. Hence, it can be expected to remove the pores in the film. Figure 6(c) depict the microstructure of a PLZT film catalysed by the use of CH_3COOH. No pores exist in this film. In fact, the function of the addition of CH_3COOH is to work as a catalyst but it also can react with the alcohol to form acetate esters (CH_3COOR'). This effect can be proven by the appearance of the characteristic band of acetate esters at around 1740 cm^{-1} in Fig. 3. The addition of CH_3COOH can contribute a chelating ligand which can react with alkoxide metal compounds to form very stable chelates, which are not easily replaced by H_2O. Hence, it can control the hydrolysis and condensation reactions that produce uniform particles; and there will be uniform shrinkage during drying which leads to high quality films. Figure 7 shows the XRD patterns of PLZT films prepared by (a) adding both the acid catalyst CH_3COOH and formamide and (b) adding only formamide. It shows that the intensity of the diffraction peaks of the perovskite phase for the sample with CH_3COOH addition is much higher than those without CH_3COOH. Therefore, the PLZT phase is much easier to form for the sample with acid catalyst addition.

Fig. 8 depicts the XRD patterns of the PLZT (8/65/35) films fired at various temperatures. A further narrowing of the peaks occurs for higher temperature

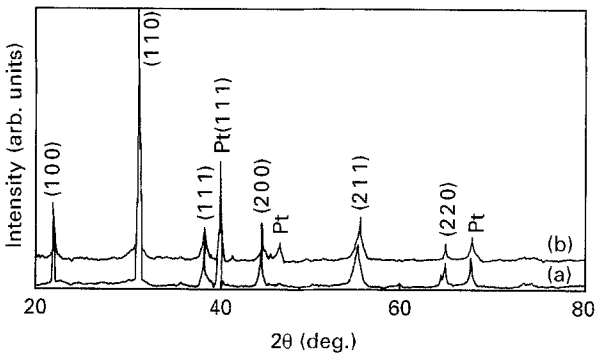

Figure 7 XRD patterns of PLZT films prepared by (a) adding acid catalyst together with DCCA formamide and (b) adding DCCA formamide only.

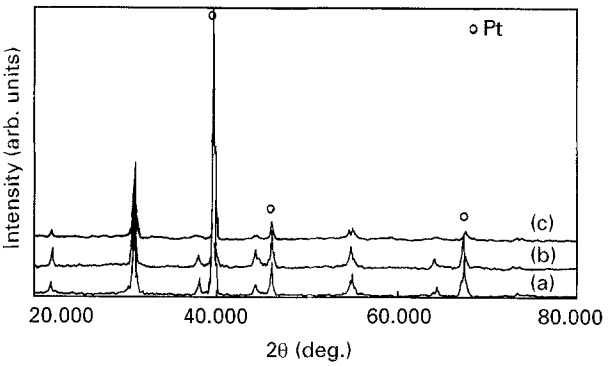

Figure 8 XRD patterns of PLZT films fired at various temperatures for 20 min. with heating rate 10 °C min^{-1}: (a) 700 °C, (b) 650 °C, (c) 600 °C.

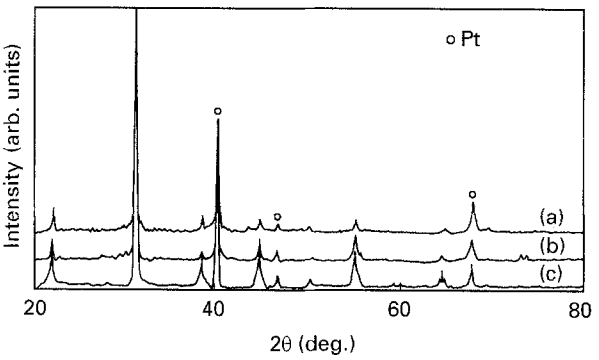

Figure 9 XRD patterns of PLZT films annealed for various times at 600 °C with heating rate 5 °C min^{-1}: (a) 0.5 h, (b) 1 h, (c) 2 h.

fired films which indicates that all the peaks shift toward higher angles as the firing temperature increases. This means that the composition and defect structure of the film are changed with increasing firing temperature. When the initial crystal nuclei formed in the films during firing they then influenced the crystallization during annealing [5].

Fig. 9 shows the XRD patterns of the films annealed for various times. It shows that the intensities of the diffraction peaks increases when the annealing time increases. This is due to that when the annealing time increases the atoms have more time or more energy to move to much better positions to form the perovskite phase.

Fig. 10 illustrates the XRD patterns of the films on the Pt/Ti/Si substrates with various thicknesses. The film thickness was established by controlling the number of coatings. The lattice constant of the substrate has more effect on the phase formation of the thinner film due to the lattice constant mismatch between the substrate and the film. This effect is expected to be

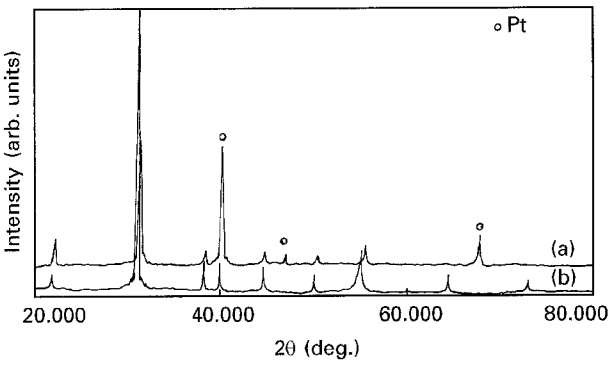

Figure 10 XRD patterns of the films on Pt/Ti/Si substrates with various thicknesses at 600 °C for 30 min. with heating rate 5 °C min^{-1}: (a) coating 5 times, (b) coating 1 time.

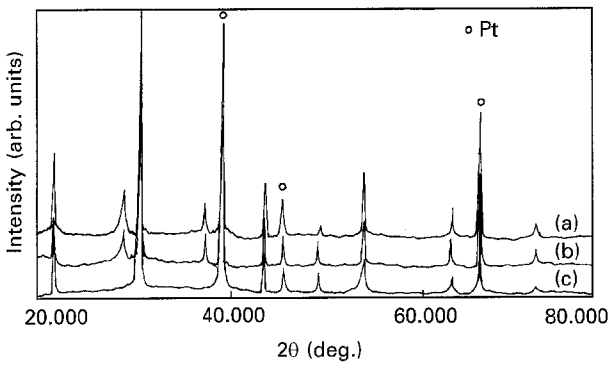

Figure 11 XRD patterns of PLZT thin films heated at various rates at 600 °C for 1 hr (a) 1 °C min^{-1}, (b) 2 °C min^{-1}, (c) 5 °C min^{-1}.

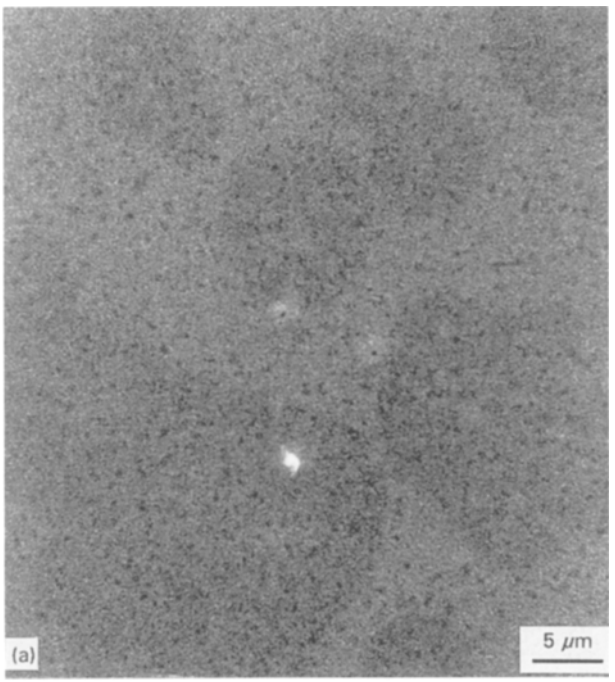

Figure 12 SEM micrographs of PLZT thin films heated for various rates at 600 °C for 1 hr (a) 1 °C min^{-1}, (b) 2 °C min^{-1}, (c) 5 °C min^{-1}.

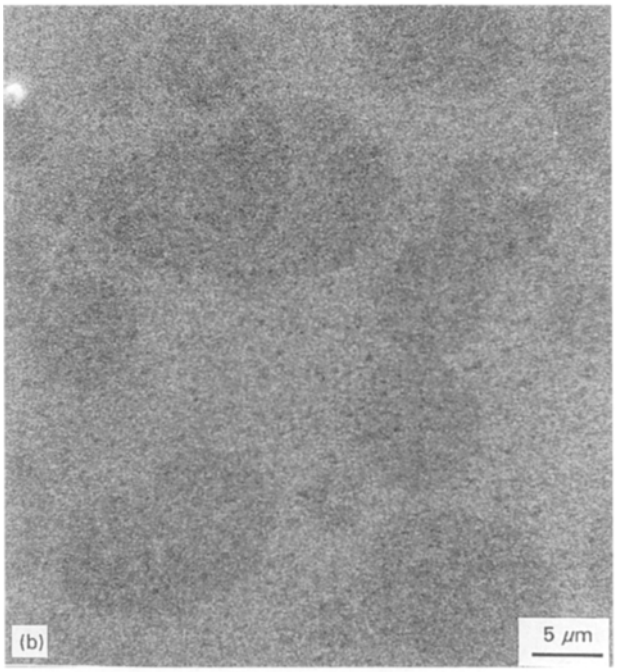

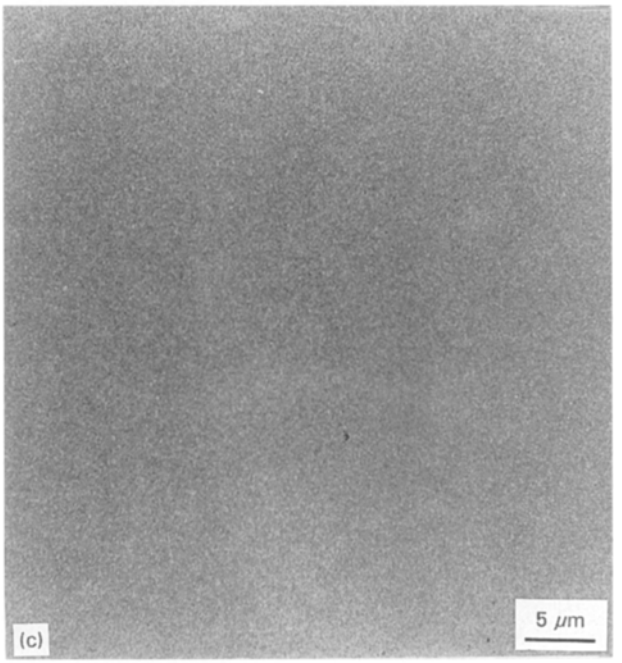

Figure 12 Continued.

decreased for thick films. The intensities of the diffraction peaks for a film produced by 5 coatings are higher than those of a film produced by one coating (Fig. 10).

Fig. 11 shows the XRD patterns of PLZT films heated at various rates. It indicates that minor amounts of a pyrochlore phase existed in the films annealed at a low heating rate. This pyrochlore phase is absent for the films annealed at higher heating rates. The reason for this difference is probably due to either an insufficient amount of oxygen or that Pb was volatilized at the higher annealing temperature. It is expected that a higher heating rate can prevent the Pb volatization and thus inhibit the forming of the pyrochlore phase [11]. If we want to obtain high quality films by the sol–gel method, it is necessary to control the conversion from the amorphous gel films to the desired crystalline phase. Fig. 12 shows the SEM

TABLE I Summary of dielectric constants of the PLZT (8/65/35) thin films.

	Dielectric constant	Thickness (μm)	Frequency (kHz)	Sintering temperature (°C)	Sintering time (min)
Swartz *et al.* [12]	200	0.4	100	700	30
Kawanno *et al.* [13]	800	2.5	10	800	120
	630	2.5	10	700	120
R. W. Vest *et al.* [14]	1800	2.5	1	650	60
Present study	540	0.350	100	600	30
	700	0.375	100	650	20
	870	0.375	1	650	20

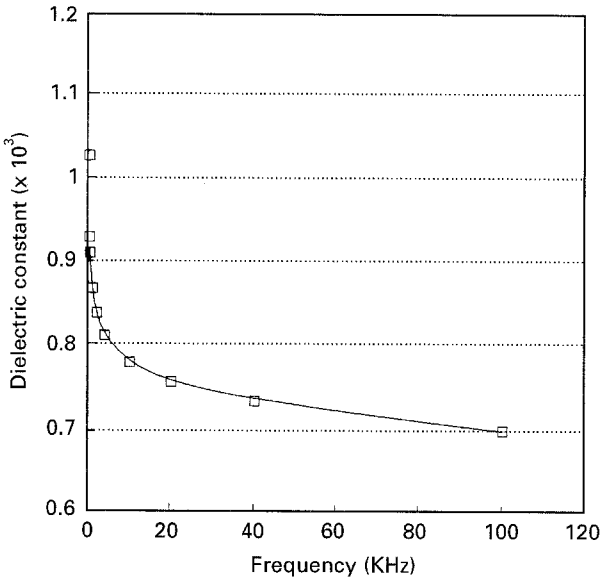

Figure 13 Dielectric constant vs. frequency curve of PLZT thin films.

micrographs of the PLZT thin films heated for various rates. It indicates that the qualities of the films prepared at low heating rate is better. Two different phases, perovskite and pyrochlore, existed in the films prepared at the low heating rate and it causes some small areas to become tarnished. Tuttle *et al.* [11] have reported that since Pb atoms have a higher density, these perovskite phases have a higher secondary electron emission yield which is consistent with the result of our XRD patterns.

The dielectric constant of the PLZT ferroelectric thin films was measured. The PLZT films were coated onto the Pt/Ti/Si substrates and Pt was used as bottom electrode. An aluminium metal film with the dimension of 0.5 mm × 1.0 mm was used as the top electrode. Fig. 13 depicts the dielectric constant versus frequency curve of a PLZT 8/65/35 thin film annealed at 650 °C for 20 min. Thin films of 0.375 μm thickness have a dielectric constant of 700 (100 KHz). The thin films annealed at 600 °C for 30 minutes have a dielectric constant of 540 (100 KHz). The polarizability, α, of the dielectric is defined by $p = \alpha E$, where p is the dipole moment induced by the local electric field, E. Basically, the dielectric constant is proportional to the polarizability of the dielectric. The total polarizability has four possible components and is given by the summation of electronic polarizability (α_e), ionic polarizability (α_i), dipolar polarizability (α_d), space charge polarizability (α_s) [15]. The magnitude of α usually decreases in the order $\alpha_s > \alpha_d > \alpha_i > \alpha_e$. At low frequencies, ($\sim 10^3$ Hz), all four (if present) may contribute to α. At radio frequencies, ($\sim 10^6$ Hz), space charge effects may not have time to build up and are effectively "relaxed out". Hence, the dielectric constant drops rapidly when the frequencies are near 1 KHz. The dielectric constants of PLZT films found from published articles are summarized in Table I. It is deduced that thin films with a high dielectric constant have been prepared by using a lower annealing temperature, a shorter annealing time and less thickness in this present study than reported by previous workers.

4. Conclusion

High quality crack- and pore-free PLZT (8/65/35) single phase thin films were successfully prepared on pt/Ti/Si substrates by sol-gel processing. The key feature of this processing was the addition of formamide and an acid catalyst into the precursor solution. The effects of the formamide and the acid catalyst on the preparation of the films were observed by IR spectra analysis. Thin films with a high dielectric constant were successfully prepared at lower temperature and shorter annealing time in this study than reported in the literature. In order to inhibit the formation of the pyrochlore phase in the films, it is necessary to anneal the films at a higher heating rate.

Acknowledgement

This study is supported by the National Science Council of R.O.C. under project No.NSC 82-0404-E009-252.

References

1. K. K. BUDD, S. K. DEY and D. A. PAYNE, *Brit. Ceram. Proc.* **36** (1985) 107.
2. L. HENCH, Science of Ceramic Chemical Processing (Wiley, New York, 1986) p. 55.
3. G. YI and M. SAYER, *Bull. Amer. Ceram. Soc.* **70** (1991) 1173.
4. D. A. CHANG, Y. H. CHOU, W. F. HSIEH, P. LIN and T. Y. TSENG, *J. Mater. Sci.* **28** (1993) 6698.
5. G. YI, Z. WU and M. SAYER, *J. Appl. Phys.* **64** (1988) 2717.

6. K. OKAZAKI and K. NAGATE, *J. Amer. Ceram. Soc.* **56** (1973) 82.
7. K. H. VON THIELE and M. PANSE, *Z. Anorg, Allg. Chem.* **440** (1978) 441.
8. A. H. BOONSTRAM, T. N. M. BERNAROS and J. I. T. SMITS, *J. Non-Cryst. Solids* **109** (1989) 141.
9. K. D. KEEFER, *Mat. Res. Soc. Symp. Proc.* **32** (1984) 15.
10. E. J. A. POPE and J. D. MacKENZIE, *J. Non-Cryst. Solids* **87** (1986) 185.
11. B. A. TUTTLE, R. W. SCHWARTZ, D. H. DOUGHTY, J. A. VOIGT and A. H. CARIM, *Mat. Res. Soc. Symp. Proc.* **200** (1990) 159.
12. S. L. SWARTZ, S. J. BRIGHT and J. R. BUSCH, *Electro Optics & Nonlinear Optics* **14** (1991) 159.
13. T. KAWANO, T. SEI and T. TSUCHIYA, *Jpn. J. Appl. Phys.* **30** (1991) 2178.
14. R. W. VEST and J. XU, *Ferroelectrics* **93** (1989) 21.
15. A. R. WEST, Solid State Chemistry and its Applications (Wiley, New York, 1986) p. 535.

Received 14 September 1994
and accepted 19 September 1995